https://doi.org/10.5194/egusphere-2026-6027
Preprint. Discussion started: 6 November 2026
© Author(s) 2026. CC BY 4.0 License.

Measurement report: Radiocarbon reveals contrasting size distributions of black carbon from fossil fuels and biomass burning in Guangzhou, China

Nannan Wei[1,2], Buqing Xu[2*], Sanyuan Zhu[2], Lingxiao Lu[2,3], Jing Li[2], Fan Jiang[4], Junwen Liu[5], Zhineng Cheng[2], Shizhen Zhao[2], Kechang Li[2], Jun Li[2], Gan Zhang[2]

1 School of Nuclear Science and Technology, University of South China, Hengyang, Hunan, 421001, China

2 State Key Laboratory of Advanced Environmental Technology, Guangzhou Institute of Geochemistry, Chinese Academy of Sciences, Guangzhou, 510640, China

3 University of Chinese Academy of Sciences, Beijing, 100049, China

4 Key Laboratory of Ecological Environment Emergency and Sudden Risk Control, South China Institute of Environmental Sciences, Ministry of Ecology and Environment, Guangzhou 510655, PR China

5 Institute for Environmental and Climate Research, College of Environment and Climate, Jinan University, Guangzhou, 511443, China

* Correspondence to:

Buqing Xu (xubuqing@gig.ac.cn)

Abstract

The size of atmospheric black carbon (BC) is a key determinant of its health and climate impacts. However, how BC sources vary with particle size remains poorly understood. We conducted radiocarbon (^{14}C)-based source apportionment of atmospheric BC in Guangzhou, China, across six discrete particle-size fractions from < 0.49 μm to 7.2–10 μm during winter and summer. The dataset comprises 81 $\Delta^{14}C$ measurements, resolving fossil-fuel and biomass-burning contributions across particle sizes. Additional $\delta^{13}C$ measurements of four representative winter sample sets were incorporated into a Bayesian model to apportion fossil-

https://doi.org/10.5194/egusphere-2026-6027
Preprint. Discussion started: 6 November 2026
© Author(s) 2026. CC BY 4.0 License.



derived BC between coal and petroleum sources. Fossil sources dominated BC, contributing 91 ± 3% in winter and 73 ± 1% in summer. In both seasons, the fossil contribution first increased and then decreased with increasing particle size, peaking in the 0.95–1.5 μm fraction (95% in winter and 88% in summer) and declining to its lowest level in the 7.2–10 μm fraction (82% in winter and 50% in summer). Coal and petroleum made comparable contributions to BC in the selected winter samples, with no consistent particle-size-dependent trends. Thus, the particle-size dependence of BC sources was driven mainly by an increasing biomass-burning contribution toward the coarse fraction, rather than by a systematic shift in the relative contributions of coal and petroleum. These findings show that bulk source fractions do not fully capture the source composition of BC across particle sizes, underscoring the need to account for source-specific size distributions when interpreting BC transport, removal, and associated climate and health effects.

1. Introduction

Black carbon (BC) is a carbonaceous aerosol produced by the incomplete combustion of fossil fuels, biomass, and waste. Owing to its strong light-absorbing capacity, BC can directly perturb the Earth's radiation balance by absorbing solar radiation and can also influence cloud formation and properties by acting as cloud condensation nuclei (Andreae and Gelencsér, 2006; Zaveri et al., 2010; Jacobson, 2004; Ramanathan and Carmichael, 2008). The climatic effects of BC are further complicated by its highly variable physical and chemical properties and by continuous changes in particle size, mixing state, and composition during atmospheric aging (Bond et al., 2013; Szopa et al., 2023). Substantial uncertainty therefore remains in quantifying the radiative forcing of BC and its contribution to both observed and projected climate change (Szopa et al., 2023; Gustafsson et al., 2026). Beyond its climatic importance, BC is also a major component of air pollution. Elevated BC concentrations can reduce atmospheric visibility and alter the thermodynamic structure of the planetary boundary layer, thereby favoring the development and persistence of haze pollution (Ding et al., 2016; Zhou et al., 2026). BC-containing particles also pose health risks and can carry toxic species, including organic

https://doi.org/10.5194/egusphere-2026-6027
Preprint. Discussion started: 6 November 2026
© Author(s) 2026. CC BY 4.0 License.

pollutants and trace metals (Ali et al., 2021; Niranjan and Thakur, 2017; Xu et al., 2026).

Particle size is an important factor controlling the atmospheric behavior and effects of BC. The size distribution of BC-containing particles reflects both their emission characteristics and subsequent atmospheric processing. After emission, BC-containing particles undergo atmospheric aging through processes such as condensation, coagulation, heterogeneous reactions, and hygroscopic growth, which continuously modify their size, morphology, mixing state, hygroscopicity, and optical properties (Oshima et al., 2009; Matsui et al., 2013). The enhanced hygroscopicity of aged BC promotes cloud condensation nuclei activation and wet scavenging, thereby affecting its atmospheric lifetime and transport (Zhou et al., 2026; Ding et al., 2019). In addition, particle size strongly influences respiratory deposition, with smaller BC particles generally penetrating more deeply into the human respiratory tract (Ching et al., 2020). However, interpreting these size-dependent behaviors and effects also requires knowledge of BC sources, because BC from different sources can differ in its initial particle properties and subsequent aging and coating development. For example, Liu et al. (2026) showed that thicker coatings on biomass-burning BC resulted in an additional radiative effect from aerosol–radiation interactions approximately two to three times that in urban environments. Characterizing the source contributions across particle-size fractions is therefore important for understanding the atmospheric evolution and climatic effects of BC and for informing assessments of human exposure to BC from different sources.

Current understanding of BC sources across different particle-size ranges remains limited. BC emitted from traffic is generally considered to have smaller particle sizes and thinner coatings than that emitted from coal and biomass combustion (Liu et al., 2019; Liu et al., 2014). Nevertheless, freshly emitted BC from these major combustion sources is predominantly distributed within the submicron range. Subsequent atmospheric ageing, particle growth, coating formation, and mixing may further alter its size distribution, leaving it unclear how BC from different sources is partitioned among discrete size fractions on the micrometre scale. Dual-carbon isotope measurements, combining $\delta^{13}C$ and $\Delta^{14}C$, provide a means of quantitatively constraining the relative contributions of the major sources of atmospheric BC

https://doi.org/10.5194/egusphere-2026-6027
Preprint. Discussion started: 6 November 2026
© Author(s) 2026. CC BY 4.0 License.

(Gustafsson et al., 2026). Previous ^{14}C-based investigations of the size dependence of BC sources have mainly relied on comparisons among PM_1, $PM_{2.5}$, and PM_{10} samples (Liu et al., 2018; Zhang et al., 2013). However, these samples represent cumulative size fractions defined by different upper cutoffs rather than discrete size intervals, and their overlapping particle-size coverage may obscure differences in BC source contributions among individual size fractions. In contrast, size-segregated sampling isolates discrete, non-overlapping particle-size intervals and allows these differences to be examined directly. To date, only a limited number of studies have applied ^{14}C analysis to the source apportionment of total carbonaceous aerosols in discrete particle-size fractions (Song et al., 2024; Angyal et al., 2024), while applications specifically targeting BC are also limited (Ni et al., 2022; Wang et al., 2013a). One such study conducted in Shanghai found no clear differences in BC source contributions among the investigated particle-size fractions; however, it included only three sets of size-segregated samples, leaving temporal and seasonal variability in size-dependent BC sources insufficiently constrained (Wang et al., 2013a).

To better understand the carbon sources of BC across particle sizes, we conducted size-resolved BC measurements in the megacity of Guangzhou, China, during winter and summer. BC sources were quantified across six discrete particle-size fractions using radiocarbon analysis, yielding a total of 81 size-resolved $\Delta^{14}C$ measurements. In addition, $\delta^{13}C$ measurements were performed for four representative winter samples to further distinguish coal and petroleum contributions within the fossil component. By combining dual-carbon isotope measurements with size-resolved source apportionment, this study aimed to address three questions: (1) Do fossil and non-fossil contributions to BC vary systematically across different particle-size fractions? (2) Do coal- and petroleum-derived BC show different size-dependent patterns within the fossil fraction? (3) How do size-dependent BC source contributions differ between winter and summer, and how might these differences relate to changes in emission conditions and monsoon-driven transport?

2. Materials and methods

2.1 Sampling

https://doi.org/10.5194/egusphere-2026-6027
Preprint. Discussion started: 6 November 2026
© Author(s) 2026. CC BY 4.0 License.

Size-segregated aerosol samples were collected using a Staplex Series 230 High Volume Cascade Impactor (Model 236, Staplex Air Sampler Division, USA), which separates particles into six aerodynamic diameter ranges (<0.49, 0.49–0.95, 0.95–1.5, 1.5–3.0, 3.0–7.2, and 7.2–10 μm). The sampler was operated at a nominal flow rate of 1.13 m^3 min^{-1} under standard conditions. Prior to field deployment, the flow rate was calibrated using a U-tube water manometer. The reference flow rate was calculated from the measured pressure difference using the Bernoulli principle and paired with the corresponding rotameter reading. A linear regression between the rotameter readings and reference flow rates was used to establish a calibration curve for flow adjustment during sampling.

Aerosol sampling was conducted at the Guangzhou Institute of Geochemistry (GIG), an urban site in Guangzhou, China (23.08°N, 113.21°E). Guangzhou is a representative urban center in the central Pearl River Delta (PRD) region (Fig. 1). The sampler was installed at approximately 30 m above ground level on the rooftop of the institute building to minimize the direct influence of local emissions. Samples were collected during two intensive campaigns covering winter (October 2021 to January 2022) and summer (July to August 2022), using pre-baked quartz fiber filters. In total, 25 size-segregated sample sets were obtained, corresponding to 150 individual filters. After sampling, all filters were wrapped in pre-baked aluminum foil, sealed, and stored at −20 °C prior to analysis.

2.2 Chemical analysis

For carbonaceous aerosol analysis, a 1.5 cm^2 punch was taken from each quartz fiber filter and analyzed for organic carbon (OC) and elemental carbon (EC). Prior to thermal–optical analysis, the filter punches were exposed to concentrated hydrochloric acid (HCl) vapor for 1 h to remove carbonate carbon and minimize its interference with the analysis (Tian et al., 2019). The OC and EC contents were quantified with a thermal–optical transmission carbon analyzer (Sunset Laboratory, Tigard, OR, USA) using the EUSAAR_2 temperature protocol (Cavalli et al., 2010). The analytical uncertainty was within ±5%, as evaluated against a sucrose standard. No detectable EC signal was observed in any of the field blanks. Although EC and BC are defined by different analytical approaches, they represent closely related light-absorbing carbonaceous

https://doi.org/10.5194/egusphere-2026-6027
Preprint. Discussion started: 6 November 2026
© Author(s) 2026. CC BY 4.0 License.

fractions, and EC is widely used as an indicator of BC in thermal–optical measurements. Hereafter, the operationally defined EC fraction is referred to as BC throughout the text.

Water-soluble inorganic ions were determined from another portion of each filter. The filter aliquots were extracted three times by ultrasonication, using 10 mL of Milli-Q water for each extraction. The combined extracts were then filtered through 0.22 μm PTFE syringe filters before instrumental analysis. Major water-soluble ions, including Na^+, NH_4^+, K^+, Mg^{2+}, Ca^{2+}, Cl^-, NO_3^-, and SO_4^{2-}, were measured by ion chromatography using a 761 Compact IC system (Metrohm, Switzerland).

2.3 Radiocarbon and stable carbon isotope analysis of BC

BC was isolated for radiocarbon analysis following our previously established method. In brief, an optimized thermal pretreatment was applied to selectively remove OC from the quartz fiber filters prior to BC combustion. This pretreatment was designed to reduce potential charring artifacts and thereby minimize the influence of OC pyrolysis on the isolated BC fraction. The residual BC on the filters was then sealed in pre-baked quartz tubes together with CuO and Ag and combusted at 900 °C to convert BC to CO_2. The resulting CO_2 was cryogenically purified on a vacuum line and subsequently converted to graphite using the hydrogen reduction method. Radiocarbon measurements were carried out at the Guangzhou Institute of Geochemistry Accelerator Mass Spectrometry facility, Chinese Academy of Sciences (GIG-AMS; 1.5 SDH-1, 0.5 MV, NEC, USA). Potential carbon contamination introduced during sample processing and measurement was evaluated using oxalic acid II (OXII; NIST) and phthalic acid (Sigma-Aldrich), as modern and fossil carbon reference materials, respectively. The radiocarbon composition of BC was determined for all winter samples and pooled summer samples, yielding a total of 81 radiocarbon measurements. For summer samples, equal-area portions of filters collected within the same month and particle-size fraction were pooled for radiocarbon analysis. Sufficient filter material was used for each radiocarbon analysis to ensure that the BC carbon mass exceeded 20 μg. In addition to radiocarbon analysis, the stable carbon isotope composition of the BC fraction in four representative winter sample sets was measured using a Flash 2000 elemental analyzer coupled to a Delta V isotope ratio mass spectrometer.

https://doi.org/10.5194/egusphere-2026-6027
Preprint. Discussion started: 6 November 2026
© Author(s) 2026. CC BY 4.0 License.

2.4 Radiocarbon-based source apportionment

Radiocarbon results were first reported as fraction modern (Fm), normalized to a common $\delta^{13}C$ value of −25 ‰. The Fm values were then converted to $\Delta^{14}C$ as follows:

$$\Delta^{14}C = (Fm \times e^{\lambda(1950-x)} - 1) \times 1000‰ \quad (1)$$

where λ is the reciprocal of the true mean life of radiocarbon (1/8267 yr^{-1}), and (x) is the year of sample collection. For the present study, (x) was set to 2021.

The radiocarbon-based fractional contributions of biomass burning ($f_{biomass}$) and fossil fuel combustion (f_{fossil} = 1- $f_{biomass}$) to BC were calculated using a two-endmember mixing model:

$$\Delta^{14}C_{sample} = f_{biomass} \times \Delta^{14}C_{biomass} + (1 - f_{biomass}) \times \Delta^{14}C_{fossil} \quad (2)$$

where $\Delta^{14}C_{sample}$ is the measured radiocarbon signature of BC, $\Delta^{14}C_{fossil}$ = −1000‰, and $\Delta^{14}C_{biomass}$ denotes $\Delta^{14}C$ endmembers of biomass burning. In this study, biomass-burning-derived BC was assumed to originate mainly from the combustion of annual plants and wood fuel. The $\Delta^{14}C$ endmember for annual plants was taken to be equivalent to atmospheric CO_2 in 2021 ($\Delta^{14}C$ = −3.5 ‰). The $\Delta^{14}C$ value of wood fuel ($\Delta^{14}C$ = 80 ‰) was estimated using a tree-growth model that included 10-, 20-, 40-, 70-, and 85-year-old trees with relative weights of 0.2, 0.2, 0.4, 0.1, and 0.1, respectively, assuming harvesting in the 2020s. Assuming equal contributions of annual plants and wood fuel to biomass-burning-derived BC in China (Wu et al., 2021; Tao et al., 2018), the $\Delta^{14}C$ endmember for biomass burning was estimated to be 38‰.

To further separate fossil-derived BC into petroleum and coal combustion contributions, the $\Delta^{14}C$ and $\delta^{13}C$ measurements were incorporated into a Bayesian Markov chain Monte Carlo (MCMC) framework (Andersson et al., 2015). The isotope mass balance can be expressed as:

$$\begin{pmatrix} \Delta^{14}C_{\text{sample}} \\ \delta^{13}C_{\text{sample}} \\ 1 \end{pmatrix} = \begin{pmatrix} \Delta^{14}C_{\text{bio}} & \Delta^{14}C_{\text{petroleum}} & \Delta^{14}C_{\text{coal}} \\ \delta^{13}C_{\text{bio}} & \delta^{13}C_{\text{petroleum}} & \delta^{13}C_{\text{coal}} \\ 1 & 1 & 1 \end{pmatrix} \cdot \begin{pmatrix} f_{\text{bio}} \\ f_{\text{petroleum}} \\ f_{\text{coal}} \end{pmatrix} \quad (3)$$

where (f) denotes the fractional contribution of each source, and the subscripts *bio*, *petroleum*, and *coal* refer to biomass burning, liquid fossil fuel combustion, and coal combustion, respectively. The isotope values labeled as "*sample*" denote measured BC isotope signatures,

https://doi.org/10.5194/egusphere-2026-6027
Preprint. Discussion started: 6 November 2026
© Author(s) 2026. CC BY 4.0 License.

whereas the source subscripts denote the corresponding isotope endmembers. The $\delta^{13}C$ and $\Delta^{14}C$ endmembers for the three source categories were compiled from previously reported datasets (Jiang et al., 2022) and are summarized in Table S1.

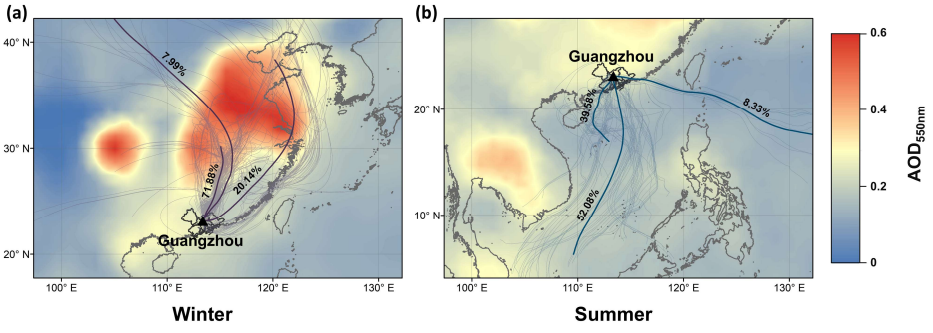


Figure 1. Mean aerosol optical depth (AOD) at 550 nm derived from the Moderate Resolution Imaging Spectroradiometer (MODIS) over East and Southeast Asia during (a) October 2021–January 2022 (winter) and (b) July–August 2022 (summer). Size-resolved aerosol samples were collected in Guangzhou (triangle), a typical urban site in the Pearl River Delta (PRD) region of South China. Five-day backward trajectories arriving at Guangzhou at an altitude of 100 m were calculated every 3 h during the sampling periods, and the corresponding mean air-mass trajectory clusters are superimposed.

3. Results and discussions

3.1 Seasonal characteristics of carbonaceous aerosols

The total concentration of carbonaceous aerosols, defined as the sum of organic matter (OM, estimated as 1.7 × OC) and BC, was approximately twofold higher in winter (27.6 ± 6.4 μg m^{-3}) than in summer (13.7 ± 4.2 μg m^{-3}). Carbonaceous aerosols accounted for 44 ± 5% of the total particulate matter (PM) mass in winter, substantially higher than the corresponding contribution in summer (17 ± 5%) (Fig. S1). In contrast, the relative contribution of water-soluble inorganic ions showed little seasonal variation, accounting for 21 ± 5% and 23 ± 7% of PM in winter and summer, respectively. Thus, the pronounced seasonal difference in PM composition was primarily associated with changes in the abundance of carbonaceous

https://doi.org/10.5194/egusphere-2026-6027
Preprint. Discussion started: 6 November 2026
© Author(s) 2026. CC BY 4.0 License.

components. The enhanced contribution of carbonaceous aerosols during winter may partly reflect the regional transport of polluted continental air masses to the PRD under the prevailing winter monsoon, as suggested by the spatial distribution of aerosol optical depth at 550 nm and the backward trajectories shown in Fig. 1.

The OC/BC ratio provides further insight into the seasonal differences in carbonaceous aerosol composition. The OC/BC ratio was substantially higher in summer (8.3 ± 2.0) than in winter (3.9 ± 0.7). This difference indicates greater summertime enrichment of OC relative to primary combustion-derived BC. Because OC/BC ratios can be affected by both primary emission profiles and secondary organic carbon (SOC) formation, the contributions of SOC and primary organic carbon (POC) were further estimated using the EC-tracer method as described in Text S1 (Castro et al., 1999). The estimated SOC contribution to OC was 67 ± 8% in summer, substantially higher than that in winter (31 ± 13%). The contrasting seasonal influences of secondary and primary organic carbon were further supported by their relationships with PM mass. During summer, PM concentrations were strongly correlated with SOC ($R^2 = 0.88$, $p < 0.01$; Fig. S2a) but not significantly correlated with POC ($p > 0.05$; Fig. S2b). In winter, PM was significantly correlated with POC ($R^2 = 0.55$, $p < 0.01$; Fig. S2d), whereas no significant correlation was observed between PM and SOC ($p > 0.05$; Fig. S2c). Together, these results indicate a greater influence of secondary organic aerosol formation during summer, whereas the wintertime carbonaceous aerosol burden was more strongly associated with primary combustion-related carbonaceous emissions (Castro et al., 1999; Duarte et al., 2008).

3.2 Size-resolved distributions and characteristics of carbonaceous aerosols

Carbonaceous aerosols were operationally grouped according to their aerodynamic diameters measured by the cascade impactor into three size fractions: submicron (<0.95 μm), accumulation (0.95–3 μm), and coarse (3–10 μm) fractions. The boundary of 0.95 μm was selected based on the transition observed in the BC size distributions. Previous studies have demonstrated that atmospheric BC is predominantly associated with submicron accumulation-mode particles, which can evolve into larger internally mixed particles during atmospheric

https://doi.org/10.5194/egusphere-2026-6027
Preprint. Discussion started: 6 November 2026
© Author(s) 2026. CC BY 4.0 License.

aging (Jia et al., 2020; Schwarz et al., 2008b). Within the operational classification adopted here, the accumulation fraction comprises the two impactor stages spanning 0.95–3.0 μm and distinguishes these particles from the smaller submicron and larger coarse fractions. Considering the size resolution and cutoff diameters of the impactor, particles larger than 3 μm were classified as coarse particles. Similar size classifications have been adopted in previous size-resolved carbonaceous aerosol studies (Xu et al., 2024; Wan et al., 2015; Song et al., 2024; Duarte et al., 2008).

The chemical composition of the three size fractions showed distinct particle-size-dependent characteristics (Fig. 2). In winter, the contribution of carbonaceous aerosols to PM decreased progressively from 55% in the submicron fraction to 28% in the coarse fraction. A similar decreasing trend was observed in summer, with the carbonaceous contribution decreasing from 27% to 9% across the same size range. In contrast, the contribution of water-soluble inorganic ions showed relatively limited variation among the three size fractions. The decreasing contribution of carbonaceous aerosols toward larger particles was therefore mainly associated with the increasing fraction of unresolved components, which likely consisted predominantly of water-insoluble mineral materials in coarse particles. These results highlight the progressive transition in particle composition from carbonaceous-rich submicron particles to increasingly mineral-influenced coarse particles, supporting the operational particle-size classification used in this study.

https://doi.org/10.5194/egusphere-2026-6027
Preprint. Discussion started: 6 November 2026
© Author(s) 2026. CC BY 4.0 License.

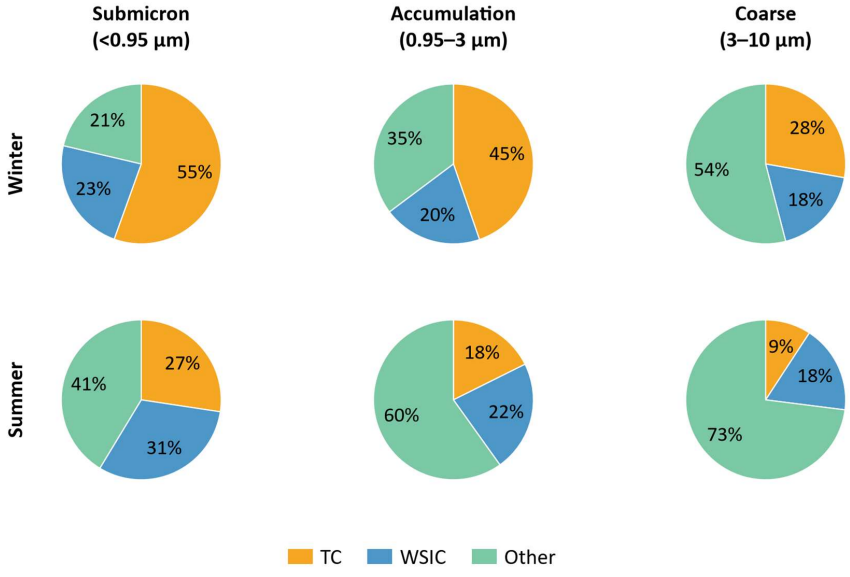


Figure 2. Mean relative contributions of total carbonaceous aerosol (TC), water-soluble inorganic ions (WSIC), and other components to particulate matter in three particle-size fractions during winter and summer. The three size fractions are defined as submicron (<0.95 µm), accumulation (0.95–3 µm), and coarse (3–10 µm) particles. TC is defined as 1.7×OC + BC. WSIC represents the sum of Cl^-, NO_3^-, SO_4^{2-}, NH_4^+, and K^+, while "Other" represents the remaining particulate mass not accounted for by TC and WSIC.

The size-normalized mass distributions of carbonaceous and inorganic species are presented in Fig. 3. BC exhibited a pronounced maximum in the 0.95–1.5 µm fraction, together with a secondary increase in the largest particle fraction (7.2–10 µm). In winter, BC was predominantly distributed in particles smaller than 3 µm, accounting for approximately 75% of total BC (Fig. S3), with a pronounced maximum in the 0.95–1.5 µm fraction (Fig. 3). Although summertime BC concentrations were substantially lower, a similar accumulation-mode peak was still observed. The enrichment of BC in the 0.95–1.5 µm fraction occurred at a larger size range than the secondary inorganic ions (SO_4^{2-} and NH_4^+), which were centered in the adjacent submicron fraction (0.49–0.95 µm) (Fig. 3). This size offset suggests that condensation of secondary species, coagulation, and aqueous-phase processing increased the aerodynamic

https://doi.org/10.5194/egusphere-2026-6027
Preprint. Discussion started: 6 November 2026
© Author(s) 2026. CC BY 4.0 License.

diameter of BC-containing particles, shifting BC toward a larger accumulation-size fraction (Jaffrezo et al., 2005; Cabada et al., 2004). In addition to the accumulation-mode maximum, a distinct increase in BC was observed in the largest particle fraction (7.2–10 μm) (Fig. 3). This coarse-mode BC enhancement occurred together with elevated Ca^{2+} and Mg^{2+} concentrations (Fig. 3), suggesting an association between coarse BC and mineral dust-related particles. Such coarse carbonaceous particles may result from the incorporation of carbonaceous materials into resuspended dust particles or the presence of carbon-containing residues associated with coarse particles. Similar coarse-mode BC peaks have also been reported in multiple Chinese urban cities (Xin et al., 2015).

Compared with BC, OC exhibited a broader but generally unimodal size distribution in both seasons, with a maximum occurring in the 0.49–1.5 μm size range (Fig. 3). This distribution partially overlapped with the size range enriched in secondary inorganic ions (SO_4^{2-} and NH_4^+), suggesting that organic components associated with secondary processing may preferentially accumulate in submicron and aging-related accumulation particles.

The OC/BC ratios exhibited contrasting size-dependent patterns between winter and summer. In winter, OC/BC ratios decreased significantly with increasing particle size (Friedman test, $p < 0.001$), from 5.0 ± 1.5 in the submicron fraction to 3.6 ± 0.9 in the accumulation fraction and 2.5 ± 0.5 in the coarse fraction (Fig. S4a). Elevated OC/BC ratios (>2) have often been used as an empirical indicator of enhanced secondary organic carbon (SOC) contributions (Turpin and Huntzicker, 1995; Chow et al., 1996). The higher OC/BC ratio in the submicron fraction likely reflects the enrichment of organic components associated with atmospheric processing and secondary organic aerosol (SOA) formation, including the condensation of oxidized organic species and aqueous-phase processing. In contrast, the lower OC/BC ratio in the coarse fraction suggests a reduced relative contribution of SOC components and an increased contribution of BC, consistent with the coarse-mode BC enhancement observed in winter (Fig. 3). In summer, OC/BC ratios showed no statistically significant differences among the three size fractions (Friedman test, $p = 0.92$, Fig. S4b). Nevertheless, OC/BC ratios were generally higher in summer than in winter across the investigated size fractions, consistent with the stronger

https://doi.org/10.5194/egusphere-2026-6027
Preprint. Discussion started: 6 November 2026
© Author(s) 2026. CC BY 4.0 License.

summertime SOC formation identified in Section 3.1. Several coarse particles exhibited exceptionally high OC/BC ratios (>20), suggesting sporadic enrichment of OC-rich components in the coarse mode. These high values may be associated with enhanced contributions from primary biological aerosol particles (PBAPs), including pollen, fungal spores, bacteria, and plant debris, which are typically enriched in coarse particles and contain abundant organic carbon (Zhu et al., 2015). The enhanced biological activity under warm and humid summertime conditions in Guangzhou may further promote the contribution of PBAPs to coarse organic carbon (Lu et al., 2025).

Overall, the contrasting size-dependent patterns of OC/BC ratios indicate distinct seasonal processes affecting BC-containing particles. However, the size distributions and relative abundances of OC and BC alone cannot determine whether these variations arise from differences in BC sources or from atmospheric processing. Therefore, size-resolved radiocarbon measurements were further applied to quantify fossil and non-fossil BC contributions and identify the dominant sources across different particle size fractions.

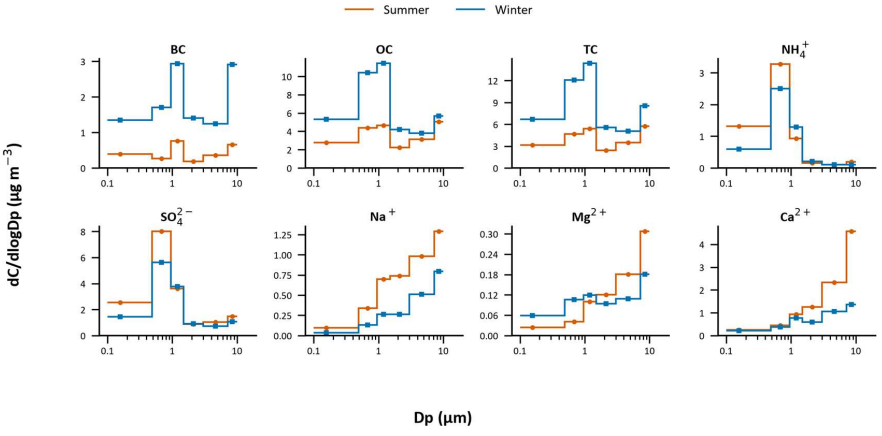


Figure 3. Size-normalized mass distributions of carbonaceous and inorganic aerosol species during summer (orange line) and winter (blue line). Carbonaceous components include black carbon (BC), organic carbon (OC), and total carbonaceous aerosol (TC). Inorganic components include NH_4^+, SO_4^{2-}, Na^+, Mg^{2+}, and Ca^{2+}. Mass concentrations were normalized by the logarithmic particle-size interval and are expressed as dC/dlogDp.

https://doi.org/10.5194/egusphere-2026-6027
Preprint. Discussion started: 6 November 2026
© Author(s) 2026. CC BY 4.0 License.

3.3 Radiocarbon (^{14}C) signatures in BC

Radiocarbon analysis revealed distinct seasonal differences in the fossil and non-fossil contributions to BC. The mass-weighted bulk $\Delta^{14}C$ values, calculated from the size-resolved measurements using an isotope mass-balance approach, were substantially lower in winter (−909 ± 34‰) than in summer (−716 ± 13‰), indicating a much larger contribution of fossil-derived BC during winter. The summertime $\Delta^{14}C$ value was comparable to previous observations in the PRD. For example, Liu et al. (2025) reported a summer BC $\Delta^{14}C$ value of −705 ± 49‰ based on measurements conducted during 2014–2018. In contrast, previous measurements in the PRD reported substantially higher wintertime BC $\Delta^{14}C$ values, including −650 ± 30‰ in 2013 (Fang et al., 2018) and −664 ± 83‰ during 2014–2018 (Liu et al., 2025), indicating a considerably larger contribution of non-fossil BC than during the winter campaign of this study. The enhanced wintertime contribution of non-fossil BC reported previously has been largely attributed to post-harvest agricultural residue burning in surrounding agricultural regions (Andersson et al., 2015; Fang et al., 2018). However, agricultural residue burning controls have been substantially strengthened in China since 2018, leading to a marked reduction in open crop burning activities and associated emissions (Hong et al., 2023). Satellite observations during our sampling periods showed substantially more fire hotspots within the PRD in summer than in winter (Fig. S5), suggesting limited regional biomass-burning activity during the winter campaign. The more ^{14}C-depleted wintertime BC observed in this study may therefore partly reflect the reduced influence of regional agricultural residue burning in recent years.

Size-resolved $\Delta^{14}C$ measurements revealed a clear particle-size dependence of BC sources in both seasons, with coarse particles consistently exhibiting higher $\Delta^{14}C$ values than submicron and accumulation particles (Fig. 4). In winter, $\Delta^{14}C$ values were highest in the largest size fraction (7.2–10 μm), followed by the 3.0–7.2 μm fraction, whereas the other four finer fractions all exhibited extremely low $\Delta^{14}C$ values (< −900‰) with no significant differences among them (Friedman test, $p = 0.44$). This contrast indicates a relatively greater non-fossil contribution to coarse BC, while the four finer fractions remained strongly dominated by fossil

https://doi.org/10.5194/egusphere-2026-6027
Preprint. Discussion started: 6 November 2026
© Author(s) 2026. CC BY 4.0 License.

sources. After combining individual size bins into three representative fractions, the wintertime coarse fraction showed a $\Delta^{14}C$ value of −837 ± 81‰, substantially higher than those of the submicron (−928 ± 40‰) and accumulation fractions (−938 ± 37‰). Despite the relatively elevated $\Delta^{14}C$ of coarse BC, the mass-weighted bulk wintertime signature remained strongly ^{14}C-depleted because most BC mass was distributed in particles smaller than 3 μm.

A similar particle-size-dependent pattern was observed in summer, but with substantially higher $\Delta^{14}C$ values across all size fractions (Fig. 4). The coarse fraction exhibited the highest $\Delta^{14}C$ value (−531 ± 29‰), whereas the submicron and accumulation fractions showed lower values, with the lowest $\Delta^{14}C$ observed in the accumulation fraction (−834 ± 14‰). Thus, although the absolute $\Delta^{14}C$ values differed substantially between seasons, both seasons exhibited a common particle-size pattern characterized by relatively ^{14}C-depleted BC in the submicron and accumulation fractions and higher $\Delta^{14}C$ values in the coarse fractions. Quantitative fossil and non-fossil source contributions and the processes underlying this size dependence are discussed in Section 3.4.

https://doi.org/10.5194/egusphere-2026-6027
Preprint. Discussion started: 6 November 2026
© Author(s) 2026. CC BY 4.0 License.

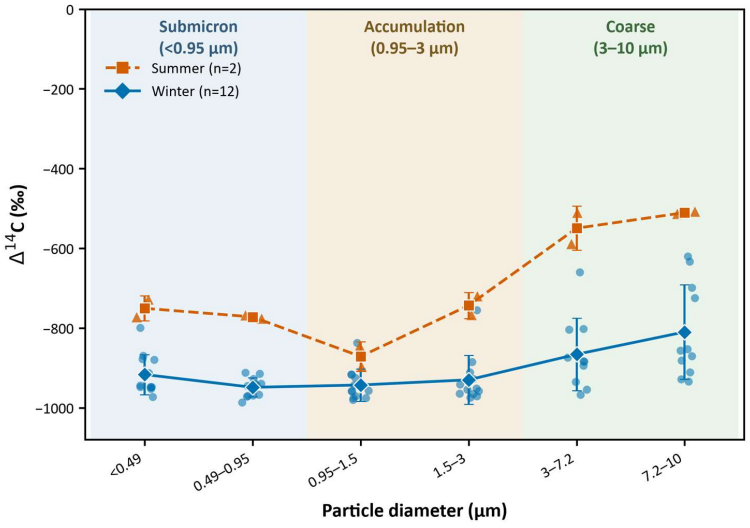


Figure 4. Size-resolved $\Delta^{14}C$ signatures of black carbon (BC) in winter and summer. Individual measurements of BC $\Delta^{14}C$ are shown as blue circles for winter and orange triangles for summer. Blue diamonds and orange squares represent the corresponding seasonal means, with error bars indicating ±1 SD. Winter measurements represent 12 samples, whereas summer measurements represent two monthly composite samples.

3.4 Size-resolved relative source contributions to BC

Radiocarbon-based source apportionment revealed that fossil fuel combustion dominated BC sources in both seasons, accounting for 91 ± 3% and 73 ± 1% of total BC in winter and summer, respectively. In terms of absolute concentrations, fossil-derived BC averaged 3.4 ± 0.9 μg m^{-3} in winter, approximately five times the summertime concentration of 0.65 ± 0.04 μg m^{-3}. In contrast, non-fossil BC concentrations differed only slightly between winter (0.32 ± 0.13 μg m^{-3}) and summer (0.25 ± 0.03 μg m^{-3}) and were comparable to the 2008–2018 average concentration in the PRD (0.34 ± 0.16 μg m^{-3}) (Liu et al., 2025). Therefore, the enhanced wintertime BC concentration was primarily driven by increased fossil-derived BC rather than enhanced non-fossil emissions. Similar seasonal variations were also reported by Fang et al. (2018), who observed that fossil BC concentrations in the PRD increased from 1.2 ± 0.1 μg m^{-3} in summer to 3.4 ± 1.5 μg m^{-3} in winter. The wintertime enhancement of fossil BC likely reflects

https://doi.org/10.5194/egusphere-2026-6027
Preprint. Discussion started: 6 November 2026
© Author(s) 2026. CC BY 4.0 License.

both the accumulation of regional emissions under a lower planetary boundary layer and reduced precipitation and the transport of fossil-fuel-related BC from continental regions under the prevailing northeasterly monsoon (Fig. 1).

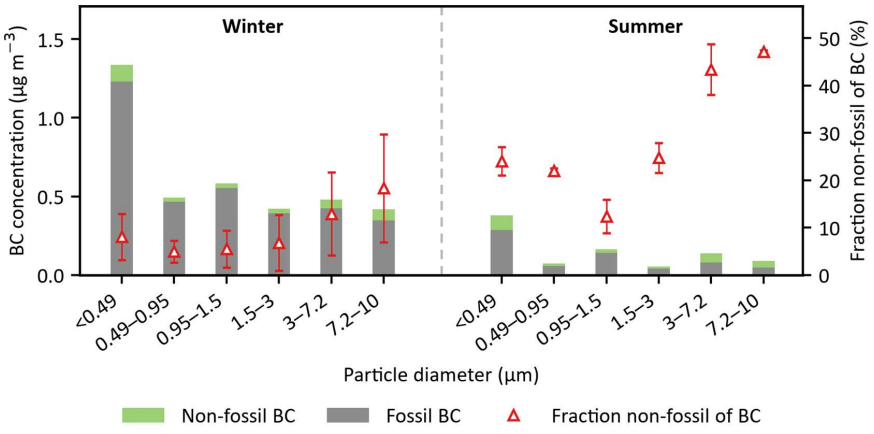
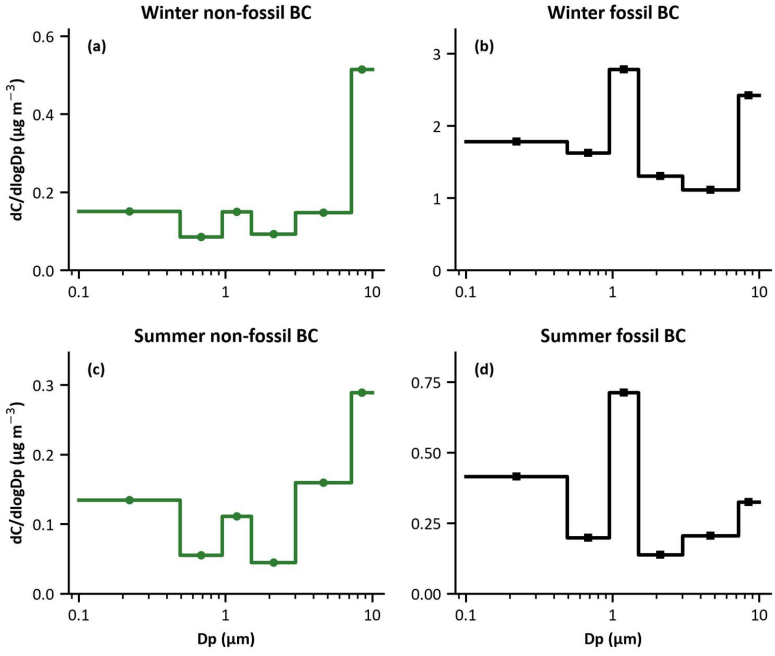


Figure 5. Size-resolved mass concentrations of fossil and non-fossil BC and the corresponding non-fossil fractions during winter and summer.

Conversion of the $\Delta^{14}C$ measurements to BC source fractions revealed a similar size-dependent pattern in both seasons, although non-fossil fractions were consistently higher in summer than in winter (Fig. 5). The non-fossil fraction was lowest in the 0.95–1.5 μm size range, accounting for 5% of BC in winter and 12% in summer, and increased markedly toward the coarse fractions. The logDp-normalized mass distributions of fossil and non-fossil BC further highlighted their contrasting particle-size patterns (Fig. 6). Both fossil and non-fossil BC exhibited unimodal size distributions in winter and summer, but with markedly different peak positions. Fossil-derived BC showed a pronounced maximum in the 0.95–1.5 μm fraction, indicating its preferential association with accumulation-mode particles. In contrast, non-fossil BC showed a pronounced coarse-mode peak in the 7.2–10 μm fraction.

https://doi.org/10.5194/egusphere-2026-6027
Preprint. Discussion started: 6 November 2026
© Author(s) 2026. CC BY 4.0 License.



400

401 **Figure 6.** Size-normalized mass distributions of non-fossil (green line) and fossil BC (black line) during winter
402 (panels a and b) and summer (panels c and d).

403 A similar tendency toward increasing biomass-burning contributions at larger particle sizes has
404 been observed in Zürich and Roveredo, Switzerland, where biomass-burning contributions
405 were higher in PM_{10} than in PM_1 during winter (Zhang et al., 2013). One possible explanation
406 for the larger particle sizes of biomass-burning-derived BC (BC_{bb}), represented here by the
407 radiocarbon-derived non-fossil BC component, is that biomass-burning emissions tend to
408 contain larger and more thickly coated BC particles than fossil-fuel combustion emissions (Liu
409 et al., 2019; Schwarz et al., 2008a). For example, previous observations showed that BC
410 particles in biomass-burning plumes had a mass median diameter of approximately 193 nm and
411 a coating thickness of 65 nm, compared with 175 nm and 20 nm, respectively, in fossil-fuel-
412 dominated plumes (Sahu et al., 2012). However, these source-dependent differences occur
413 primarily within the submicron size range and therefore cannot directly explain the pronounced
414 enrichment of BC_{bb} observed in the 7.2–10 µm fraction. Moreover, coarse-mode enrichment of
415 BC_{bb} is not a general feature, even in regions strongly influenced by biomass burning, such as

https://doi.org/10.5194/egusphere-2026-6027
Preprint. Discussion started: 6 November 2026
© Author(s) 2026. CC BY 4.0 License.

Southeast and South Asia. In Thailand, BC_{bb} decreased with increasing particle size, with 70–90% of total BC_{bb} distributed in $PM_{1.1}$ (Song et al., 2024). Similarly, measurements in the Maldives showed that the fossil contribution to BC was higher in total suspended particles (50 ± 4%) than in $PM_{2.5}$ (41 ± 4%), implying a relatively greater fossil-fuel contribution to the coarse fraction (Bosch et al., 2014). These contrasting observations suggest that the coarse-mode enrichment of non-fossil BC in the PRD cannot be explained solely by source-dependent differences in the initial size and coating of emitted BC particles but likely also involves region-specific transport and mixing processes.

The relationships of BC_{bb} with biomass-burning and mineral-dust tracers provide further insight into its enrichment in coarse particles. In the 7.2–10 μm fraction, BC_{bb} was significantly correlated with Ca^{2+} in both winter and summer (R^2 = 0.73 and 0.83, respectively) (Fig. 7a and Fig. 7c), whereas no significant correlations were observed in the other size fractions ($p > 0.05$). BC_{bb} was also strongly correlated with nss-K^+, a typical inorganic tracer of biomass burning (Fig. 7b and Fig. 7d). The significant correlations of BC_{bb} with both nss-K^+ and Ca^{2+} are consistent with an association between biomass-burning BC and mineral particles in the coarse fraction, potentially resulting from their mixing during regional transport. Mineral dust can provide surfaces for the coagulation and mixing of combustion-derived aerosols with coarse particles during atmospheric transport, thereby promoting the incorporation of BC into the coarse fraction (Clarke et al., 2004). Such BC–dust mixing has also been observed directly in transported mineral-dust plumes and urban aerosols (Zhou et al., 2018; Kandler et al., 2007; Mahfouz et al., 2024).

https://doi.org/10.5194/egusphere-2026-6027
Preprint. Discussion started: 6 November 2026
© Author(s) 2026. CC BY 4.0 License.

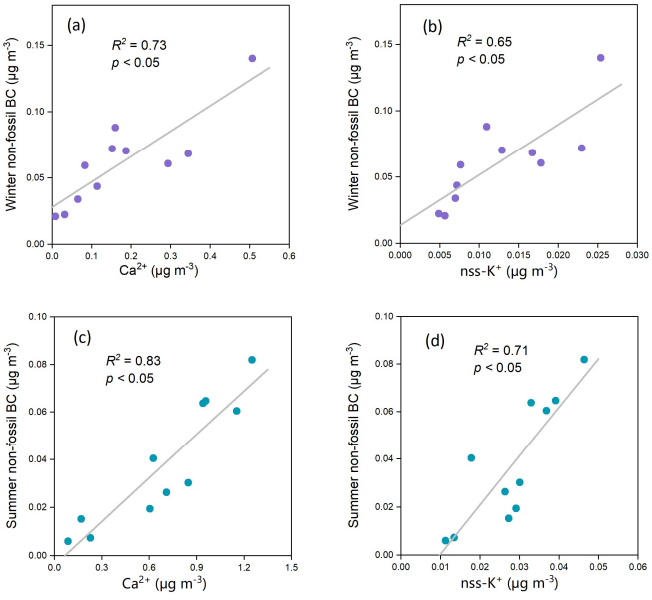


Figure 7. Correlations of non-fossil BC concentrations with Ca^{2+} and non-sea-salt K^+ (nss-K^+) in the coarse fraction (7.2–10 μm) during winter and summer. Panels (a) and (b) show the relationships for winter samples, whereas panels (c) and (d) show those for summer samples.

The coarse-mode enrichment of BC_{bb} was substantially more pronounced in summer than in winter. Biomass burning contributed approximately 50% of BC in the 7.2–10 μm fraction during summer, compared with 16 ± 8% during winter (Fig. 5). This seasonal pattern is somewhat unexpected because biomass-burning activities in southern China generally intensify during the colder winter period (Lu et al., 2025). The elevated summertime BC_{bb} contribution therefore appears unlikely to result primarily from stronger local or regional biomass-burning emissions within southern China but instead points to a change in the dominant source regions and transport pathways. Long-range transport from Southeast Asia may represent an important contributor to summertime BC_{bb}. Biomass burning accounts for approximately 50–80% of BC in parts of Southeast Asia (Wang et al., 2023; Liu et al., 2020), substantially higher than the generally <30% contribution reported for East Asia. Previous studies have further demonstrated that Southeast Asian biomass-burning aerosols can be transported into southern China and the PRD under the summer monsoon circulation (Lu et al., 2025; Qin et al., 2024). More recently,

https://doi.org/10.5194/egusphere-2026-6027
Preprint. Discussion started: 6 November 2026
© Author(s) 2026. CC BY 4.0 License.

a radiocarbon-constrained modeling study estimated that transport from Southeast Asia contributed approximately 26% of BC_{bb} in the PRD during the summer monsoon, with contributions reaching as high as 66% during individual transport episodes (Lin et al., 2026). Notably, that modeling study covered summer 2022, overlapping with the present sampling campaign and thereby providing temporally relevant support for the potential influence of Southeast Asian transport on our observations. In contrast, the wintertime northeasterly monsoon predominantly transports continental air masses from mainland China, which are more strongly influenced by fossil-fuel-derived BC (Fig. 1). Thus, the pronounced summertime enrichment of BC_{bb} in coarse particles likely reflects the combined effects of Southeast Asian biomass-burning emissions, monsoon-driven transport, and mixing of BC_{bb} with coarse mineral particles during regional transport.

Whereas BC_{bb} showed a pronounced enrichment in the coarse fraction, fossil-derived BC (BC_{ff}) exhibited the opposite size-dependent pattern and was preferentially concentrated in the accumulation fraction. The fossil contribution to BC was highest in the accumulation fraction (Fig. 5), and the logDp-normalized BC_{ff} distribution showed a pronounced peak at 0.95–1.5 μm (Fig. 6). This enrichment is likely related to the atmospheric growth of initially finer fossil-fuel-derived BC particles. After emission, BC-containing particles can grow through water uptake, coagulation, condensation of secondary inorganic and organic material, and heterogeneous reactions, progressively shifting BC mass toward the accumulation mode (Fierce et al., 2015; Huang et al., 2012). Such aging-related growth may be particularly important for fossil-derived BC. Fossil-fuel BC is generally emitted as relatively small and less-coated particles, and its comparatively slow transition toward highly hygroscopic states may reduce its initial susceptibility to wet removal, allowing a larger fraction to remain in the atmosphere and undergo continued aging and particle growth (Subramanian et al., 2010; Moteki et al., 2007; Shiraiwa et al., 2007). In contrast, BC_{bb} is often emitted with thicker coatings and can become hydrophilic more rapidly, resulting in more efficient removal through cloud activation and precipitation scavenging during transport (Qi and Wang, 2019; Akagi et al., 2012). This difference in atmospheric evolution and removal pathways may contribute to the preferential

https://doi.org/10.5194/egusphere-2026-6027
Preprint. Discussion started: 6 November 2026
© Author(s) 2026. CC BY 4.0 License.

enrichment of BC_{ff} in the 0.95–1.5 μm fraction. Consistent with this interpretation, the OC/BC ratio in the 0.95–1.5 μm fraction showed a positive relationship with the fossil fraction during winter (R^2 = 0.54, p < 0.05, Fig. S6). Because increasing OC/BC ratios can reflect organic enrichment and atmospheric processing, their positive association with the fossil fraction suggests that fossil-derived BC became progressively enriched as BC-containing particles underwent atmospheric aging and grew into the accumulation mode.

3.5 Fossil BC apportioned by stable carbon isotopes: coal versus liquid fossil fuel

Stable carbon isotope measurements provided additional constraints on the size-dependent sources of BC in four representative winter samples. The coarse fraction exhibited a slightly more negative $\delta^{13}C$ value (−24.1 ± 0.7‰) than the submicron (−23.1 ± 1.3‰) and accumulation fractions (−23.0 ± 1.3‰), although the differences among the three size fractions were not statistically significant (one-way ANOVA, p > 0.05). In $\delta^{13}C$–$\Delta^{14}C$ space, coarse particles tended to exhibit more negative $\delta^{13}C$ and higher $\Delta^{14}C$ values, consistent with their greater non-fossil contribution and the increased influence of biomass-burning-derived BC (Fig. S7). In contrast, the submicron and accumulation fractions showed largely overlapping dual-isotope signatures, indicating similar source characteristics dominated by fossil-derived BC. Because $\delta^{13}C$ provides additional discrimination between coal and liquid fossil-fuel combustion, the dual-carbon isotope measurements were further incorporated into a Bayesian MCMC model to separate the major BC sources.

The Bayesian MCMC model estimated the relative contributions of biomass burning (f_{bb}), coal combustion (f_{coal}), and liquid petroleum combustion (f_{petrol}) to BC for four representative wintertime samples (Fig. 8). After weighting the source fractions by BC mass across the six size fractions, the average contributions of biomass burning, coal combustion, and liquid petroleum combustion were 9 ± 4%, 49 ± 5%, and 42 ± 8%, respectively. Overall, coal and petroleum combustion made comparable contributions to wintertime BC in the PRD, consistent with previous observations in the region. For example, the average contributions of coal and petroleum combustion to BC in the PRD during 2008–2018 were 38 ± 2% and 35 ± 2%, respectively (Liu et al., 2025).

https://doi.org/10.5194/egusphere-2026-6027
Preprint. Discussion started: 6 November 2026
© Author(s) 2026. CC BY 4.0 License.

Despite the comparable overall contribution of f_{coal} and f_{petrol}, the two fossil sources differed among the four samples. The f_{coal} values exceeded f_{petrol} in October and November, whereas f_{petrol} was slightly higher than f_{coal} in December and January (Fig. 8a). These sample-to-sample differences were observed across nearly all particle-size fractions, suggesting that temporal changes in source influence affected the entire BC size distribution rather than a particular size fraction (Yang et al., 2017). Backward trajectories showed that the October and November samples were associated with longer-range air masses traced to northern and northeastern mainland China (Fig. S8a and Fig. S8b), consistent with a stronger influence of continental transport and coal-related BC emissions in northern China. In contrast, the December and January samples were characterized by shorter trajectories and more stagnant conditions, with air masses entering the PRD directly from the southeastern coastal region (Fig. S8c and Fig. S8d), favoring a greater influence of local and regional liquid-petroleum-related sources. These results suggest that liquid-fossil-fuel-derived BC in the PRD was more closely associated with local and regional urban emissions, particularly traffic emissions, whereas northerly continental transport increased the influence of coal-derived BC.

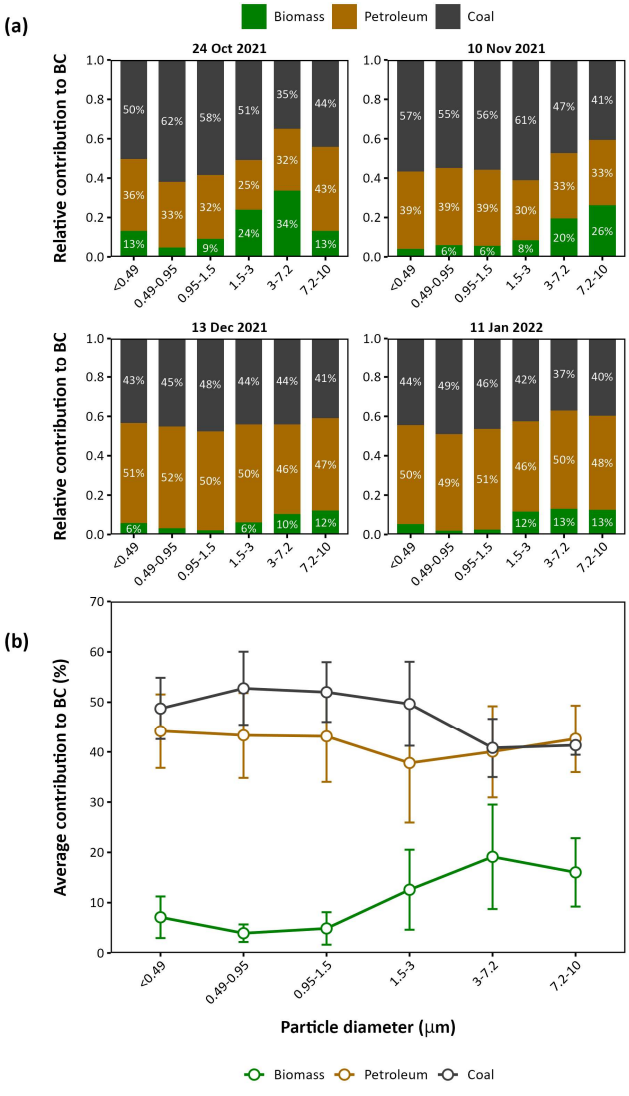
Unlike the sample-to-sample differences described above, the particle-size dependence of the two fossil-source contributions was comparatively weak. Within individual samples, f_{coal} and f_{petrol} showed only limited variation across particle-size fractions, particularly for samples collected in December and January (Fig. 8a). Although this result is based on only four winter samples, it suggests that atmospheric processing, including coating, coagulation, and mixing, did not preferentially redistribute coal- and petroleum-derived BC among the investigated particle-size fractions. In contrast, the most remarkable size-dependent change in the Bayesian source fractions was associated with biomass burning rather than with the relative contributions of the two fossil sources. The mean f_{bb} increased from < 10% in the submicron and accumulation fractions to 10–20% in the coarse fractions, whereas f_{coal} and f_{petrol} generally remained at approximately 40–50% across the investigated size fractions (Fig. 8b). Thus, the shift in BC source composition toward larger particle sizes was driven mainly by an increasing biomass-burning contribution rather than by changes in the relative contributions of the two

https://doi.org/10.5194/egusphere-2026-6027
Preprint. Discussion started: 6 November 2026
© Author(s) 2026. CC BY 4.0 License.

fossil sources.

The absence of a systematic increase in f_{coal} toward the coarse fractions contrasts with the particle-size patterns expected from primary fossil-fuel combustion. Coal combustion has often been associated with relatively larger BC-containing particles than vehicle exhaust emissions, and a greater contribution of coal-derived BC might therefore be expected in the coarse fraction (Bosch et al., 2014). For example, a size-resolved study in Shanghai reported that fossil-derived BC in particles larger than 3 μm was almost exclusively attributed to coal combustion (Wang et al., 2013b). In the PRD, however, no corresponding increase in fcoal was observed in the coarse fraction, where fcoal and fpetrol remained comparable (Fig. 8b). One possible explanation is that coarse fossil BC in the PRD includes carbonaceous particles from non-combustion sources, particularly carbon-black-containing tire wear that is subsequently incorporated into resuspended road dust (Zhang et al., 2013; Kim et al., 2021; Järlskog et al., 2022; Reynolds et al., 2024). Such particles would be identified as fossil-derived by $\Delta^{14}C$ but may not be adequately represented by the combustion-derived $\delta^{13}C$ endmembers used in the Bayesian model. Therefore, the apportioned coal and petroleum contributions in the coarse fractions should not necessarily be interpreted exclusively as direct combustion emissions.

https://doi.org/10.5194/egusphere-2026-6027
Preprint. Discussion started: 6 November 2026
© Author(s) 2026. CC BY 4.0 License.



554

555 **Figure 8.** Size-resolved source contributions to BC derived from dual-carbon isotope constrained Bayesian source
556 apportionment for four representative winter samples. (a) Relative contributions of biomass burning, petroleum
557 combustion, and coal combustion to BC across six particle-size fractions. (b) Mean source contributions for each
558 particle-size fraction across the four samples. Error bars represent the standard deviations among the four samples.

559 **4. Conclusion**

560 This study investigated the sources and size distributions of black carbon (BC) in Guangzhou,

https://doi.org/10.5194/egusphere-2026-6027
Preprint. Discussion started: 6 November 2026
© Author(s) 2026. CC BY 4.0 License.

China, using size-resolved radiocarbon (^{14}C) and stable carbon isotope (^{13}C) measurements. BC was strongly dominated by fossil sources, which contributed 91 ± 3% in winter and 73 ± 1% in summer. In both seasons, the highest fossil fractions occurred in the 0.95–1.5 μm size range, reaching 95% in winter and 88% in summer, whereas the non-fossil contribution increased markedly toward the coarse fraction and reached approximately 50% in the largest size range (7.2–10 μm) during summer. The logDp-normalized mass distribution of fossil-derived BC (BC_{ff}) peaked in the 0.95–1.5 μm fraction, whereas that of biomass-burning-derived BC (BC_{bb}) peaked in the 7.2–10 μm fraction. In the 7.2–10 μm fraction, BC_{bb} was strongly correlated with nss-K^+ and Ca^{2+}, consistent with an association between biomass-burning BC and coarse mineral particles, potentially resulting from their mixing during regional transport. In contrast, the accumulation-mode peak of BC_{ff} suggests that initially finer fossil-derived BC particles may grow through atmospheric processing and shift into the accumulation mode. Within the fossil fraction, coal and petroleum combustion made comparable contributions in the four representative winter samples, and neither source contribution exhibited a consistent particle-size-dependent trend. Thus, the particle-size dependence of BC sources was driven mainly by an increasing biomass-burning contribution toward the coarse fraction, rather than by a systematic shift between the two fossil sources.

However, size-resolved sampling yields only a small mass of BC in each particle-size fraction, making it difficult to measure both $\delta^{13}C$ and $\Delta^{14}C$. We therefore quantified the relative contributions of coal and petroleum in only four winter sample sets with high BC loadings. How these contributions vary across particle sizes in other seasons remains unclear. A further uncertainty concerns the contribution of non-exhaust traffic emissions, including particles from tire wear and asphalt pavement wear. These emissions have received increasing attention as potential sources of urban BC (Järlskog et al., 2022), but their isotopic endmembers remain poorly characterized. We therefore did not include them as separate sources in the apportionment model. Finally, isotope measurements on bulk material from each size fraction cannot directly resolve the mixing state of individual particles. Nevertheless, the contrasting size distributions of BC from fossil fuels and biomass burning show that bulk source fractions

https://doi.org/10.5194/egusphere-2026-6027
Preprint. Discussion started: 6 November 2026
© Author(s) 2026. CC BY 4.0 License.

can obscure differences in source contributions across particle sizes. This distinction is important for understanding the sources, transport, and removal of BC aerosols and for assessing their climate, environmental, and health impacts.

Data Availability Statement

Data described in this manuscript can be accessed at https://doi.org/10.5281/zenodo.23239332 (Xu, 2026). The aerosol optical depth data are available through the Moderate Resolution Imaging Spectroradiometer (MODIS) observations (https://giovanni.gsfc.nasa.gov/giovanni/). The isentropic backward airmass trajectories are available through the NOAA Air Resources Laboratory (http://ready.arl.noaa.gov/HYSPLIT.php).

Author Contributions

NW and BX conceived the study. NW and Jing Li collected the samples. NW performed the chemical analysis with the support of FJ and JWL. ZC and SYZ carried out the radiocarbon measurements. BX interpreted the data and drafted the paper. LL contributed to figure preparation. GZ and Jun Li provided funding. All co-authors provided input on the interpretations and early versions of the paper.

Conflict of Interest

The authors declare no conflicts of interest relevant to this study.

Acknowledgments

This work is supported by the National Natural Science Foundation of China (42192511), Guangdong Provincial Applied Science and Technology Research and Development Program (2023B0303000007), and Natural Science Foundation of Guangdong Province, China (No. 2023A1515011301).

References:

Akagi, S. K., Craven, J. S., Taylor, J. W., McMeeking, G. R., Yokelson, R. J., Burling, I. R., Urbanski, S. P., Wold, C. E., Seinfeld, J. H., Coe, H., Alvarado, M. J. & Weise, D. R.: Evolution of trace gases and particles emitted by a chaparral fire in California, Atmos. Chem. Phys., 12, 1397-1421, 10.5194/acp-12-1397-2012, 2012.

https://doi.org/10.5194/egusphere-2026-6027
Preprint. Discussion started: 6 November 2026
© Author(s) 2026. CC BY 4.0 License.



Ali, M. U., Siyi, L., Yousaf, B., Abbas, Q., Hameed, R., Zheng, C., Kuang, X. & Wong, M. H.: Emission sources and full spectrum of health impacts of black carbon associated polycyclic aromatic hydrocarbons (PAHs) in urban environment: A review, Crit. Rev. Environ. Sci. Technol., 51, 857-896, 10.1080/10643389.2020.1738854, 2021.

Andersson, A., Deng, J., Du, K., Zheng, M., Yan, C., Skold, M. & Gustafsson, O.: Regionally-varying combustion sources of the January 2013 severe haze events over eastern China, Environ. Sci. Technol., 49, 2038-43, 10.1021/es503855e, 2015.

Andreae, M. O. & Gelencsér, A.: Black carbon or brown carbon? The nature of light-absorbing carbonaceous aerosols, Atmos. Chem. Phys., 6, 3131-3148, 10.5194/acp-6-3131-2006, 2006.

Angyal, A., Szoboszlai, Z., Major, I., Molnár, M., Varga, T., Török, Z., Papp, E., Enikő, F., Gini, M., Manousakas, M. I., Szikszai, Z. & Kertész, Z.: Characterisation of urban aerosol size distribution by radiocarbon and PIXE analyses in a middle-European urban environment for source identification: a pilot study, Environ. Sci. Pollut. Res., 31, 47258-47274, 10.1007/s11356-024-34215-8, 2024.

Bond, T. C., Doherty, S. J., Fahey, D. W., Forster, P. M., Berntsen, T., DeAngelo, B. J., Flanner, M. G., Ghan, S., Kärcher, B., Koch, D., Kinne, S., Kondo, Y., Quinn, P. K., Sarofim, M. C., Schultz, M. G., Schulz, M., Venkataraman, C., Zhang, H., Zhang, S., Bellouin, N., Guttikunda, S. K., Hopke, P. K., Jacobson, M. Z., Kaiser, J. W., Klimont, Z., Lohmann, U., Schwarz, J. P., Shindell, D., Storelvmo, T., Warren, S. G. & Zender, C. S.: Bounding the role of black carbon in the climate system: A scientific assessment, J. Geophys. Res. Atmos., 118, 5380-5552, https://doi.org/10.1002/jgrd.50171, 2013.

Bosch, C., Andersson, A., Kirillova, E. N., Budhavant, K., Tiwari, S., Praveen, P. S., Russell, L. M., Beres, N. D., Ramanathan, V. & Gustafsson, Ö.: Source-diagnostic dual-isotope composition and optical properties of water-soluble organic carbon and elemental carbon in the South Asian outflow intercepted over the Indian Ocean, Journal of Geophysical Research: Atmospheres, 119, 11,743-11,759, 10.1002/2014jd022127, 2014.

Cabada, J. C., Rees, S., Takahama, S., Khlystov, A., Pandis, S. N., Davidson, C. I. & Robinson, A. L.: Mass size distributions and size resolved chemical composition of fine particulate matter at the Pittsburgh supersite, Atmos. Environ., 38, 3127-3141, https://doi.org/10.1016/j.atmosenv.2004.03.004, 2004.

Castro, L. M., Pio, C. A., Harrison, R. M. & Smith, D. J. T.: Carbonaceous aerosol in urban and rural European atmospheres: estimation of secondary organic carbon concentrations, Atmos. Environ., 33, 2771-2781, https://doi.org/10.1016/S1352-2310(98)00331-8, 1999.

Cavalli, F., Viana, M., Yttri, K. E., Genberg, J. & Putaud, J. P.: Toward a standardised thermal-optical protocol for measuring atmospheric organic and elemental carbon: the EUSAAR protocol, Atmos. Meas. Tech., 3, 79-89, 10.5194/amt-3-79-2010, 2010.

Ching, J., Kajino, M. & Matsui, H.: Resolving aerosol mixing state increases accuracy of black carbon respiratory deposition estimates, One Earth, 3, 763-776, 10.1016/j.oneear.2020.11.004, 2020.

Chow, J. C., Watson, J. G., Lu, Z., Lowenthal, D. H., Frazier, C. A., Solomon, P. A., Thuillier, R. H. & Magliano, K.: Descriptive analysis of PM2.5 and PM10 at regionally representative locations during SJVAQS/AUSPEX, Atmos. Environ., 30, 2079-2112, https://doi.org/10.1016/1352-2310(95)00402-5, 1996.

Clarke, A. D., Shinozuka, Y., Kapustin, V. N., Howell, S., Huebert, B., Doherty, S., Anderson, T., Covert,

https://doi.org/10.5194/egusphere-2026-6027
Preprint. Discussion started: 6 November 2026
© Author(s) 2026. CC BY 4.0 License.

D., Anderson, J., Hua, X., Moore II, K. G., McNaughton, C., Carmichael, G. & Weber, R.: Size distributions and mixtures of dust and black carbon aerosol in Asian outflow: Physiochemistry and optical properties, J. Geophys. Res.: Atmos., 109, https://doi.org/10.1029/2003JD004378, 2004.

Ding, A. J., Huang, X., Nie, W., Sun, J. N., Kerminen, V.-M., Petäjä, T., Su, H., Cheng, Y. F., Yang, X.-Q., Wang, M. H., Chi, X. G., Wang, J. P., Virkkula, A., Guo, W. D., Yuan, J., Wang, S. Y., Zhang, R. J., Wu, Y. F., Song, Y., Zhu, T., Zilitinkevich, S., Kulmala, M. & Fu, C. B.: Enhanced haze pollution by black carbon in megacities in China, Geophys. Res. Lett., 43, 2873-2879, https://doi.org/10.1002/2016GL067745, 2016.

Ding, S., Zhao, D., He, C., Huang, M., He, H., Tian, P., Liu, Q., Bi, K., Yu, C., Pitt, J., Chen, Y., Ma, X., Chen, Y., Jia, X., Kong, S., Wu, J., Hu, D., Hu, K., Ding, D. & Liu, D.: Observed Interactions Between Black Carbon and Hydrometeor During Wet Scavenging in Mixed-Phase Clouds, Geophys. Res. Lett., 46, 8453-8463, https://doi.org/10.1029/2019GL083171, 2019.

Duarte, R. M. B. O., Mieiro, C. L., Penetra, A., Pio, C. A. & Duarte, A. C.: Carbonaceous materials in size-segregated atmospheric aerosols from urban and coastal-rural areas at the Western European Coast, Atmos. Res., 90, 253-263, https://doi.org/10.1016/j.atmosres.2008.03.003, 2008.

Fang, W., Du, K., Andersson, A., Xing, Z., Cho, C., Kim, S.-W., Deng, J. & Gustafsson, Ö.: Dual-Isotope Constraints on Seasonally Resolved Source Fingerprinting of Black Carbon Aerosols in Sites of the Four Emission Hot Spot Regions of China, J. Geophys. Res.: Atmos., 123, 11,735-11,747, 10.1029/2018jd028607, 2018.

Fierce, L., Riemer, N. & Bond, T. C.: Explaining variance in black carbon's aging timescale, Atmos. Chem. Phys., 15, 3173-3191, 10.5194/acp-15-3173-2015, 2015.

Gustafsson, Ö., Budhavant, K., Chimurkar, N., Clarke, S., Dreyfus, G., Gong, X., Klimont, Z., Klingmü ller, K., Kim, S.-W., Lelieveld, J., Myhre, G., Nair, H. R. C. R., Peng, J., Ramanathan, V., Rana, A., Manoj, M. R., Satheesh, S. K., Venkataraman, C. & Zhang, Q.: Atmospheric black carbon in the climate system, Nat. Rev. Earth Environ., 7, 312-328, 10.1038/s43017-026-00773-3, 2026.

Hong, X., Zhang, C., Tian, Y., Wu, H., Zhu, Y. & Liu, C.: Quantification and evaluation of atmospheric emissions from crop residue burning constrained by satellite observations in China during 2016–2020, Sci Total Environ., 865, 161237, https://doi.org/10.1016/j.scitotenv.2022.161237, 2023.

Huang, X.-F., Sun, T.-L., Zeng, L.-W., Yu, G.-H. & Luan, S.-J.: Black carbon aerosol characterization in a coastal city in South China using a single particle soot photometer, Atmos. Environ., 51, 21-28, https://doi.org/10.1016/j.atmosenv.2012.01.056, 2012.

Jacobson, M. Z.: Climate response of fossil fuel and biofuel soot, accounting for soot's feedback to snow and sea ice albedo and emissivity, J. Geophys. Res. Atmos., 109, https://doi.org/10.1029/2004JD004945, 2004.

Jaffrezo, J. L., Aymoz, G. & Cozic, J.: Size distribution of EC and OC in the aerosol of Alpine valleys during summer and winter, Atmos. Chem. Phys., 5, 2915-2925, 10.5194/acp-5-2915-2005, 2005.

Järlskog, I., Jaramillo-Vogel, D., Rausch, J., Perseguers, S., Gustafsson, M., Strömvall, A.-M. & Andersson-Sköld, Y.: Differentiating and Quantifying Carbonaceous (Tire, Bitumen, and Road Marking Wear) and Non-carbonaceous (Metals, Minerals, and Glass Beads) Non-exhaust Particles in Road Dust Samples from a Traffic Environment, Water Air Soil Pollut., 233, 375, 10.1007/s11270-022-05847-8, 2022.

Jia, S., Zhang, Q., Sarkar, S., Mao, J., Hang, J., Chen, W., Wang, X., Yuan, L., Yang, L., Ye, G. & Zhou, S.: Size-segregated deposition of atmospheric elemental carbon (EC) in the human respiratory

https://doi.org/10.5194/egusphere-2026-6027
Preprint. Discussion started: 6 November 2026
© Author(s) 2026. CC BY 4.0 License.

system: A case study of the Pearl River Delta, China, Sci Total Environ., 708, 134932, https://doi.org/10.1016/j.scitotenv.2019.134932, 2020.

Jiang, F., Liu, J., Cheng, Z., Ding, P., Xu, Y., Zong, Z., Zhu, S., Zhou, S., Yan, C., Zhang, Z., Zheng, J., Tian, C., Li, J. & Zhang, G.: Dual-carbon isotope constraints on source apportionment of black carbon in the megacity Guangzhou of the Pearl River Delta region, China for 2018 autumn season, Environ. Pollut., 294, 118638, https://doi.org/10.1016/j.envpol.2021.118638, 2022.

Kandler, K., Benker, N., Bundke, U., Cuevas, E., Ebert, M., Knippertz, P., Rodríguez, S., Schütz, L. & Weinbruch, S.: Chemical composition and complex refractive index of Saharan Mineral Dust at Izaña, Tenerife (Spain) derived by electron microscopy, Atmos. Environ., 41, 8058-8074, https://doi.org/10.1016/j.atmosenv.2007.06.047, 2007.

Kim, J., Yang, S. I., Moon, H., Hong, J., Hong, J., Choi, W., Son, H., Lee, B.-c., Kim, G.-B. & Kim, Y.: Potential release of nano-carbon black from tire-wear particles through the weathering effect, J. Ind. Eng. Chem., 96, 322-329, https://doi.org/10.1016/j.jiec.2021.01.036, 2021.

Lin, B., Jiang, H., Li, J., Li, T., Zhang, Z., Tang, J., Zhu, S., Cheng, Z., Geng, X., Mo, Y., Li, J., Jiang, H., Chen, D. & Zhang, G.: Inventory Uncertainty and Transboundary Transport of Biomass-Burning Black Carbon in Southern China: Insights from Combining Radiocarbon Measurements with Modeling, Environ. Sci. Technol., 10.1021/acs.est.6c00449 2026.

Liu, D., Allan, J. D., Young, D. E., Coe, H., Beddows, D., Fleming, Z. L., Flynn, M. J., Gallagher, M. W., Harrison, R. M., Lee, J., Prevot, A. S. H., Taylor, J. W., Yin, J., Williams, P. I. & Zotter, P.: Size distribution, mixing state and source apportionment of black carbon aerosol in London during wintertime, Atmos. Chem. Phys., 14, 10061-10084, 10.5194/acp-14-10061-2014, 2014.

Liu, D., Jiang, F., Hu, K., Ding, S., Wang, X., Wu, H., Yang, Y., Zheng, Z., Yu, C., Allan, J., Hu, D., Sun, Y., Tian, P., Zhao, D., Huang, M., Li, S., Wu, Y., Kompalli, S. K., Suresh Babu, S., Li, W., Bi, L., Kong, S., Wang, Y., Chen, Y., Liu, P., Schwarz, J. P. & Coe, H.: Warming potential of atmospheric black carbon modulated by particulate matter, Nat. Geosci., 10.1038/s41561-026-02068-0, 2026.

Liu, D., Joshi, R., Wang, J., Yu, C., Allan, J. D., Coe, H., Flynn, M. J., Xie, C., Lee, J., Squires, F., Kotthaus, S., Grimmond, S., Ge, X., Sun, Y. & Fu, P.: Contrasting physical properties of black carbon in urban Beijing between winter and summer, Atmos. Chem. Phys., 19, 6749-6769, 10.5194/acp-19-6749-2019, 2019.

Liu, J., Andersson, A., Zhong, G., Geng, X., Ding, P., Zhu, S., Cheng, Z., Zakaria, M. P., Bong, C. W., Li, J., Zheng, J., Zhang, G. & Gustafsson, O.: Isotope constraints of the strong influence of biomass burning to climate-forcing Black Carbon aerosols over Southeast Asia, Sci Total Environ., 744, 140359, 10.1016/j.scitotenv.2020.140359, 2020.

Liu, J., Ding, P., Zong, Z., Li, J., Tian, C., Chen, W., Chang, M., Salazar, G., Shen, C., Cheng, Z., Chen, Y., Wang, X., Szidat, S. & Zhang, G.: Evidence of Rural and Suburban Sources of Urban Haze Formation in China: A Case Study From the Pearl River Delta Region, J. Geophys. Res.: Atmos., 123, 4712-4726, https://doi.org/10.1029/2017JD027952, 2018.

Liu, J., Jiang, F., Wang, Q., Zhang, G., Li, J., Chen, W., Ding, P., Zhu, S., Cheng, Z., Zhang, X., Sha, Q., Huang, Z., Yuan, X., Zheng, J., Zhang, Y., Yan, C., Tian, C., Chen, Y., Yu, J. Z. & Gustafsson, Ö.: Substantial reductions in black carbon from both fossil fuels and biomass burning during China's Clean Air Action, Proc. Natl. Acad. Sci. U.S.A., 122, e2500843122, doi:10.1073/pnas.2500843122, 2025.

Lu, L., Xu, B., Kunwar, B., Pokhrel, A., Kawamura, K. & Zhang, G.: Temporal Variations and Source

https://doi.org/10.5194/egusphere-2026-6027
Preprint. Discussion started: 6 November 2026
© Author(s) 2026. CC BY 4.0 License.

Apportionment of Biomass Burning and Biogenic Organic Aerosols in the Pearl River Delta: Effects of the Monsoon, Plant Phenology, and Anthropogenic Activities, J. Geophys. Res.: Atmos., 130, e2024JD042625, https://doi.org/10.1029/2024JD042625, 2025.

Mahfouz, M. M. K., Skok, G., Sciare, J., Pikridas, M., Alfarra, M. R., Moosakutty, S., Alfoldy, B., Ivančič, M., Rigler, M., Gregorič, A., Podlipec, R., Lohmann, S., Hlawacek, G., Heller, R., Tutsak, E. & Močnik, G.: Contribution of black carbon and desert dust to aerosol absorption in the atmosphere of the Eastern Arabian Peninsula, Atmos. Environ., 324, 120427, https://doi.org/10.1016/j.atmosenv.2024.120427, 2024.

Matsui, H., Koike, M., Kondo, Y., Moteki, N., Fast, J. D. & Zaveri, R. A.: Development and validation of a black carbon mixing state resolved three-dimensional model: Aging processes and radiative impact, J. Geophys. Res. Atmos., 118, 2304-2326, https://doi.org/10.1029/2012JD018446, 2013.

Moteki, N., Kondo, Y., Miyazaki, Y., Takegawa, N., Komazaki, Y., Kurata, G., Shirai, T., Blake, D. R., Miyakawa, T. & Koike, M.: Evolution of mixing state of black carbon particles: Aircraft measurements over the western Pacific in March 2004, Geophys. Res. Lett., 34, https://doi.org/10.1029/2006GL028943, 2007.

Ni, H., Huang, R.-J., Yao, P., Cosijn, M. M., Kairys, N., Zhong, H. & Dusek, U.: Organic aerosol formation and aging processes in Beijing constrained by size-resolved measurements of radiocarbon and stable isotopic 13C, Environ. Int., 158, 106890, https://doi.org/10.1016/j.envint.2021.106890, 2022.

Niranjan, R. & Thakur, A. K.: The Toxicological Mechanisms of Environmental Soot (Black Carbon) and Carbon Black: Focus on Oxidative Stress and Inflammatory Pathways, Front. Immunol., 8, 10.3389/fimmu.2017.00763, 2017.

Oshima, N., Koike, M., Zhang, Y. & Kondo, Y.: Aging of black carbon in outflow from anthropogenic sources using a mixing state resolved model: 2. Aerosol optical properties and cloud condensation nuclei activities, J. Geophys. Res. Atmos., 114, https://doi.org/10.1029/2008JD011681, 2009.

Qi, L. & Wang, S.: Fossil fuel combustion and biomass burning sources of global black carbon from GEOS-Chem simulation and carbon isotope measurements, Atmos. Chem. Phys., 19, 11545-11557, 10.5194/acp-19-11545-2019, 2019.

Qin, Y., Wang, H., Wang, Y., Lu, X., Tang, H., Zhang, J., Li, L. & Fan, S.: Wildfires in Southeast Asia pollute the atmosphere in the northern South China Sea, Sci. Bull., 69, 1011-1015, https://doi.org/10.1016/j.scib.2024.02.026, 2024.

Ramanathan, V. & Carmichael, G.: Global and regional climate changes due to black carbon, Nat. Geosci., 1, 221-227, 10.1038/ngeo156, 2008.

Reynolds, R. L., Molden, N., Kokaly, R. F., Lowers, H., Breit, G. N., Goldstein, H. L., Williams, E. K., Lawrence, C. R. & Derry, J.: Microplastic and Associated Black Particles From Road-Tire Wear: Implications for Radiative Effects Across the Cryosphere and in the Atmosphere, J. Geophys. Res. Atmos., 129, e2024JD041116, https://doi.org/10.1029/2024JD041116, 2024.

Sahu, L. K., Kondo, Y., Moteki, N., Takegawa, N., Zhao, Y., Cubison, M. J., Jimenez, J. L., Vay, S., Diskin, G. S., Wisthaler, A., Mikoviny, T., Huey, L. G., Weinheimer, A. J. & Knapp, D. J.: Emission characteristics of black carbon in anthropogenic and biomass burning plumes over California during ARCTAS-CARB 2008, J. Geophys. Res. Atmos., 117, https://doi.org/10.1029/2011JD017401, 2012.

Schwarz, J. P., Gao, R. S., Spackman, J. R., Watts, L. A., Thomson, D. S., Fahey, D. W., Ryerson, T. B.,

https://doi.org/10.5194/egusphere-2026-6027
Preprint. Discussion started: 6 November 2026
© Author(s) 2026. CC BY 4.0 License.



Peischl, J., Holloway, J. S., Trainer, M., Frost, G. J., Baynard, T., Lack, D. A., de Gouw, J. A., Warneke, C. & Del Negro, L. A.: Measurement of the mixing state, mass, and optical size of individual black carbon particles in urban and biomass burning emissions, Geophys. Res. Lett., 35, https://doi.org/10.1029/2008GL033968, 2008a.

Schwarz, J. P., Spackman, J. R., Fahey, D. W., Gao, R. S., Lohmann, U., Stier, P., Watts, L. A., Thomson, D. S., Lack, D. A., Pfister, L., Mahoney, M. J., Baumgardner, D., Wilson, J. C. & Reeves, J. M.: Coatings and their enhancement of black carbon light absorption in the tropical atmosphere, J. Geophys. Res.: Atmos., 113, https://doi.org/10.1029/2007JD009042, 2008b.

Shiraiwa, M., Kondo, Y., Moteki, N., Takegawa, N., Miyazaki, Y. & Blake, D. R.: Evolution of mixing state of black carbon in polluted air from Tokyo, Geophys. Res. Lett., 34, https://doi.org/10.1029/2007GL029819, 2007.

Song, W., Hong, Y., Zhang, Y., Cao, F., Rauber, M., Santijitpakdee, T., Kawichai, S., Prapamontol, T., Szidat, S. & Zhang, Y.-L.: Biomass Burning Greatly Enhances the Concentration of Fine Carbonaceous Aerosols at an Urban Area in Upper Northern Thailand: Evidence From the Radiocarbon-Based Source Apportionment on Size-Resolved Aerosols, J. Geophys. Res.: Atmos., 129, e2023JD040692, https://doi.org/10.1029/2023JD040692, 2024.

Subramanian, R., Kok, G. L., Baumgardner, D., Clarke, A., Shinozuka, Y., Campos, T. L., Heizer, C. G., Stephens, B. B., de Foy, B., Voss, P. B. & Zaveri, R. A.: Black carbon over Mexico: the effect of atmospheric transport on mixing state, mass absorption cross-section, and BC/CO ratios, Atmos. Chem. Phys., 10, 219-237, 10.5194/acp-10-219-2010, 2010.

Szopa, S., Naik, V., Adhikary, B., Artaxo, P., Berntsen, T., Collins, W. D., Fuzzi, S., Gallardo, L., Kiendler-Scharr, A. & Klimont, Z. 2023. Short-Lived Climate Forcers (Chapter 6). In *IPCC : Climate Change : The Physical Science Basis. Contribution of Working Group I to the Sixth Assessment Report of the Intergovernmental Panel on Climate Change.* , 817-922. Cambridge University Press.

Tao, S., Ru, M. Y., Du, W., Zhu, X., Zhong, Q. R., Li, B. G., Shen, G. F., Pan, X. L., Meng, W. J., Chen, Y. L., Shen, H. Z., Lin, N., Su, S., Zhuo, S. J., Huang, T. B., Xu, Y., Yun, X., Liu, J. F., Wang, X. L., Liu, W. X., Cheng, H. F. & Zhu, D. Q.: Quantifying the rural residential energy transition in China from 1992 to 2012 through a representative national survey, Nat. Energy, 3, 567-573, 10.1038/s41560-018-0158-4, 2018.

Tian, S., Pan, Y., Liu, Z., Wen, T. & Wang, Y.: Reshaping the size distribution of aerosol elemental carbon by removal of coarse mode carbonates, Atmos. Environ., 214, 116852, https://doi.org/10.1016/j.atmosenv.2019.116852, 2019.

Turpin, B. J. & Huntzicker, J. J.: Identification of secondary organic aerosol episodes and quantitation of primary and secondary organic aerosol concentrations during SCAQS, Atmos. Environ., 29, 3527-3544, https://doi.org/10.1016/1352-2310(94)00276-Q, 1995.

Wan, X., Kang, S., Wang, Y., Xin, J., Liu, B., Guo, Y., Wen, T., Zhang, G. & Cong, Z.: Size distribution of carbonaceous aerosols at a high-altitude site on the central Tibetan Plateau (Nam Co Station, 4730ma.s.l.), Atmos. Res., 153, 155-164, https://doi.org/10.1016/j.atmosres.2014.08.008, 2015.

Wang, G.-h., Zeng, Y.-s., Yao, J., Qian, Y., Huang, Y., Liu, K., Liu, W. & Li, Y.: Source apportionment of atmospheric carbonaceous particulate matter based on the radiocarbon, J. Radioanal. Nucl. Chem., 295, 1545-1552, 10.1007/s10967-012-2245-5, 2013a.

Wang, G., Yao, J., Zeng, Y., Huang, Y., Qian, Y., Liu, W., Li, Y., Yuan, N., Liu, S. & Shan, J.: Source

https://doi.org/10.5194/egusphere-2026-6027
Preprint. Discussion started: 6 November 2026
© Author(s) 2026. CC BY 4.0 License.

Apportionment of Carbonaceous Particulate Matter in a Shanghai Suburb Based on Carbon Isotope Composition, Aerosol Sci. Technol., 47, 239-248, 10.1080/02786826.2012.743959, 2013b.

Wang, X., Li, J., Zhang, X., Cheng, Z., Jiang, H., Jiang, H., Lin, B., Zhu, S., Zhao, S., Liu, J., Tian, C., Zhang, R. & Zhang, G.: An innovative passive sampler to reveal the high contribution of biomass burning to black carbon over Indo-China Peninsula: Radiocarbon constraints, Atmos. Environ., 294, 119522, https://doi.org/10.1016/j.atmosenv.2022.119522, 2023.

Wu, J., Kong, S., Zeng, X., Cheng, Y., Yan, Q., Zheng, H., Yan, Y., Zheng, S., Liu, D., Zhang, X., Fu, P., Wang, S. & Qi, S.: First High-Resolution Emission Inventory of Levoglucosan for Biomass Burning and Non-Biomass Burning Sources in China, Environ. Sci. Technol., 55, 1497-1507, 10.1021/acs.est.0c06675, 2021.

Xin, J., Wang, Y., Pan, Y., Ji, D., Liu, Z., Wen, T., Wang, Y., Li, X., Sun, Y. & Sun, J.: The campaign on atmospheric aerosol research network of China: CARE-China, Bull. Am. Meteorol. Soc., 96, 1137-1155, 10.1175/BAMS-D-14-00039.1, 2015.

Xu, B.: Zenodo [data set], https://doi.org/10.5281/zenodo.23239332, 2026

Xu, H., Zhang, W., Zheng, S., Dai, R., Meng, W., Zhu, Y., Wang, J., Zhong, Q., Shen, H., Shen, G., Ma, J. & Tao, S.: The Hidden Health and Climate Burden of Black Carbon under China's Dual Carbon Strategy, Nat. Commun., 10.1038/s41467-026-77632-8, 2026.

Xu, M., Hu, B., Zhao, S., Yan, G., Wen, T. & Zhao, X.: Size-resolved water-soluble organic carbon and its significant contribution to aerosol liquid water, Sci Total Environ., 927, 172396, https://doi.org/10.1016/j.scitotenv.2024.172396, 2024.

Yang, Y., Wang, H., Smith, S. J., Ma, P. L. & Rasch, P. J.: Source attribution of black carbon and its direct radiative forcing in China, Atmos. Chem. Phys., 17, 4319-4336, 10.5194/acp-17-4319-2017, 2017.

Zaveri, R. A., Barnard, J. C., Easter, R. C., Riemer, N. & West, M.: Particle-resolved simulation of aerosol size, composition, mixing state, and the associated optical and cloud condensation nuclei activation properties in an evolving urban plume, J. Geophys. Res.: Atmos., 115, https://doi.org/10.1029/2009JD013616, 2010.

Zhang, Y. L., Zotter, P., Perron, N., Prévôt, A. S. H., Wacker, L. & Szidat, S.: Fossil and non-fossil sources of different carbonaceous fractions in fine and coarse particles by radiocarbon measurement, Radiocarbon, 55, 1510-1520, 10.1017/S0033822200048438, 2013.

Zhou, D., Ding, K., Huang, X., Liu, L., Liu, Q., Xu, Z., Jiang, F., Fu, C. & Ding, A.: Transport, mixing and feedback of dust, biomass burning and anthropogenic pollutants in eastern Asia: a case study, Atmos. Chem. Phys., 18, 16345-16361, 10.5194/acp-18-16345-2018, 2018.

Zhou, Q., Wang, S., Bie, S., Cai, J., Chen, Y., Cheng, Y., Ding, X., Gu, J., Li, J., Li, W., Liu, D., Liu, J., Liu, Y., Shang, J., Tang, X., Tang, R., Tian, Y., Wang, J., Wang, S., Wei, J., Wei, Y., Xiang, Y., Yan, C., Zhang, F., Zhang, Z., Zhang, G., Zhang, Q., Zhang, Y., Zhong, G. & Zheng, M.: A review of atmospheric black carbon research progress in China, Atmos. Environ., 383, 122290, https://doi.org/10.1016/j.atmosenv.2026.122290, 2026.

Zhu, C., Kawamura, K. & Kunwar, B.: Organic tracers of primary biological aerosol particles at subtropical Okinawa Island in the western North Pacific Rim, J. Geophys. Res.: Atmos., 120, 5504-5523, 10.1002/2015jd023611, 2015.